Vietnam Journal of Science and Technology ***62*** *(1) (2024) 170-183*

doi:10.15625/2525-2518/18622

A new method of failure analysis

Sergei Alexandrov[1, 2], Marina Rynkovskaya[2, *], Ismet Bajmuratov[2], Ruslan Kalistratov[2], Ivan Pylkin[2]

[1]*Ishlinsky Institute for Problems in Mechanics RAS, 101-1 Prospect Vernadskogo, Moscow 119526, Russia*

[2]*Department of Civil Engineering, Peoples' Friendship University of Russia named after Patrice Lumumba (RUDN University), 6 Miklukho-Maklaya Str., Moscow 117198, Russia*

[*]Email: *rynkovskaya-mi@rudn.ru*

Received: 5 August 2023; Accepted for publication: 24 October 2023

Abstract. The present paper develops a new failure analysis method under plane strain conditions considering a generalized linear yield criterion. The yield criterion and the stress equilibrium equations constitute a hyperbolic system of equations. It is shown that two auxiliary variables satisfy the equation of telegraphy. Simple analytical relationships connect these variables and the radii of curvature of the characteristic curves. The calculated radii of curvature allow the corresponding characteristic net to be constructed. Then, the stress field is determined using another set of analytical relationships. Thus, a numerical procedure is only necessary for solving the equation of telegraphy. This equation can be integrated by the method of Riemann. In particular, Green's function is the Bessel function of zero order. A simple example illustrates the general method.

Keywords: linear yield criterion, plane strain, telegraph equation, failure.

Classification numbers: 5.4.3, 5.4.6.

1. INTRODUCTION

The application of stress-based yield (or failure) criteria requires a stress analysis of structures. In the case of statically determinate problems, a yield criterion and the stress equilibrium equations can be solved independently of the other constitutive equations. The present paper deals with such statically determinate systems under plane strain conditions, assuming a generalized linear yield criterion. The study is restricted to hyperbolic systems of equations.

Several methods are available for determining stress fields in metal plasticity based on pressure-independent yield criteria. In all cases, the methods aim at determining characteristic nets. The corresponding stress fields are then found using simple relationships. One of these methods derives the equations for the radii of curvature of characteristic lines [1]. It has been shown that these radii satisfy separately the equation of telegraphy. This method is usually referred to as the *R* - *S* method. Another method was proposed by Mikhlin and is sometimes named the method of moving coordinates [2, 3]. This method introduces a Cartesian coordinate system whose axes are tangent to characteristic lines at each point of a region. The moving

coordinates also satisfy the equation of telegraphy. The third method derives the equations for principal line coordinates. The coordinate lines of principal line coordinate systems coincide with principal stress trajectories. The starting point of this method is the simple relationship between the scale factors of the principal line coordinates derived in [4]. As in the previous methods, the equation of telegraphy should be solved for calculating characteristic nets.

Many materials obey pressure-dependent yield criteria, for example, soils, granular materials, porous and powder metals, and concrete. The most widely used yield criterion for such materials is that of Mohr-Coulomb [5 - 8]. Modified versions of this criterion are also often used for various materials [9 - 12]. Other piecewise linear yield criteria have been proposed and used in [13 - 15], among many others.

The methods above have been extended to various linear yield criteria (i.e., the criteria represented by linear equations in terms of the principal stresses). The *R* – *S* method has been extended to the Mohr-Coulomb yield criterion in [16] and the piecewise linear yield criterion proposed in [13] in [17]. The method of moving coordinates has been generalized on the Mohr-Coulomb yield criterion in [18] and a generalized linear yield criterion in [19]. The method based on the geometric properties of principal line coordinates has been developed in [20] for the Mohr-Coulomb yield criterion and [21] for a generalized linear yield criterion.

It depends on the specific boundary value problem which of the above methods is most convenient. For example, using the moving coordinates method to calculate the stress field near curved traction-free surfaces is advantageous [3, 19, 22]. However, it is worth noting that all the methods apply in a region where both families of characteristics are curved. On the other hand, in many cases, such a region is adjacent to a region where one of the characteristic families is straight. In such cases, the *R* - *S* method is most advantageous. The present paper develops the *R*- *S* method for a generalized linear yield criterion. Thus, it generalizes one of the most used methods for solving boundary value problems in plane-strain plasticity on any linear yield criterion that results in a system of hyperbolic equations.

2. SYSTEM OF EQUATIONS

The phrase ‘piecewise linear yield criterion’ is usually referred to a yield criterion that is represented by linear functions of the principal stresses. Under plane strain conditions, the general piecewise linear criterion is

$$q\sigma_1 - \sigma_2 = \sigma_0, \tag{1}$$

where σ_1 and σ_2 are the principal stresses in the planes of flow, σ_0 is a reference stress, and q is constant. It is assumed without loss of generality that

$$\sigma_1 > \sigma_2. \tag{2}$$

The equations comprising (1) and the stress equilibrium equations are hyperbolic if $q > 0$ [2]. The present paper is restricted to this case. This section briefly describes the characteristic analysis to introduce the equations required for subsequent derivation.

The characteristic directions are inclined at an angle ϕ to the direction of σ_1 (Figure 1). This angle is determined as

$$\phi = \arctan\sqrt{q}. \tag{3}$$

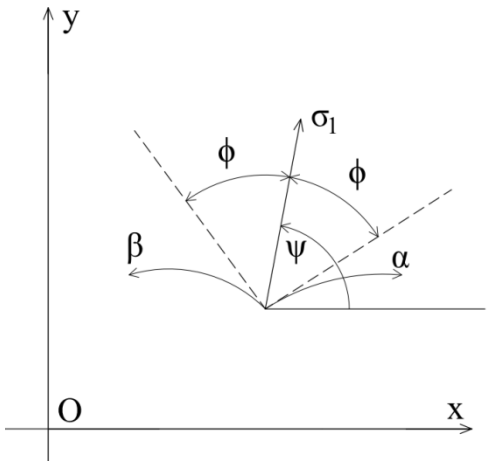

Figure 1. Characteristic and Cartesian coordinates.

The two families of characteristics are regarded as the coordinate lines of a curvilinear coordinate system (α, β). The line of action of σ_1 falls in the sector between the positive directions of these coordinate lines (Figure 1). Introduce a Cartesian coordinate system (x, y). Let ψ be the angle between the x-axis and the direction of σ_1, measured from the axis anticlockwise. Then, the equations of the $\alpha-$ and $\beta-$ lines are

$$\frac{dy}{dx} = \tan(\psi - \phi) \text{ and } \frac{dy}{dx} = \tan(\psi + \phi), \tag{4}$$

respectively. The characteristic relations are

$$\begin{aligned} &d\sigma_1 - \frac{\left[(1-q)\sigma_1 - \sigma_0\right]}{\sqrt{q}} d\psi = 0 \qquad \text{along} \quad \text{an } \alpha-\text{line}, \\ &d\sigma_1 + \frac{\left[(1-q)\sigma_1 - \sigma_0\right]}{\sqrt{q}} d\psi = 0 \qquad \text{along} \quad \text{a } \beta-\text{line}. \end{aligned} \tag{5}$$

These equations can be rewritten as

$$\begin{aligned} &d\Lambda - d\psi = 0 \qquad \text{along} \quad \text{an } \alpha-\text{line}, \\ &d\Lambda + d\psi = 0 \qquad \text{along} \quad \text{a } \beta-\text{line}, \end{aligned} \tag{6}$$

where

$$\Lambda = \frac{\sqrt{q}}{(1-q)} \ln\left[(1-q)\frac{\sigma_1}{\sigma_0} + 1\right]. \tag{7}$$

In a region where both families of characteristics are curved, the equations in (6) can be represented as

$$\Lambda - \psi = -2\mu\beta + \Lambda_0 \text{ and } \Lambda + \psi = 2\mu\alpha + \Lambda_0. \tag{8}$$

Here μ is a constant whose value will be specified later, and Λ_0 is a constant of integration. Solving the equations in (8) for Λ and ψ, one gets

$$\Lambda - \Lambda_0 = \mu(\alpha - \beta) \text{ and } \psi = \mu(\alpha + \beta). \tag{9}$$

3. METHOD OF CALCULATING CHARACTERISTIC NETS

Equations (1), (7), and (9) allow the stress field to be found if a characteristic net is determined. A method of calculating characteristic nets is developed in this section.

The radii of curvature of the $\alpha-$ and $\beta-$ lines are denoted as *R* and *S*, respectively. It is seen from (3) that the angle between each characteristic direction and the line of action of the stress σ_1 is constant. Therefore, the radii of curvature of the characteristic curves can be defined by the following equations:

$$\frac{1}{R} = \frac{\partial \psi}{\partial s_\alpha} \text{ and } \frac{1}{S} = -\frac{\partial \psi}{\partial s_\beta}, \tag{10}$$

where $\partial / \partial s_\alpha$ and $\partial / \partial s_\beta$ are space derivatives taken along the $\alpha-$ and $\beta-$ lines, respectively. It follows from the geometry of Figure 1 that

$$\begin{aligned} \frac{\partial x}{\partial s_\alpha} &= \cos(\psi - \phi), \quad \frac{\partial x}{\partial s_\beta} = \cos(\psi + \phi), \\ \frac{\partial y}{\partial s_\alpha} &= \sin(\psi - \phi), \quad \frac{\partial y}{\partial s_\beta} = \sin(\psi + \phi). \end{aligned} \tag{11}$$

Using (9) and (10), one can transform (11) to

$$\begin{aligned} \frac{\partial x}{\partial \alpha} &= \mu R \cos(\psi - \phi), \quad \frac{\partial x}{\partial \beta} = -\mu S \cos(\psi + \phi), \\ \frac{\partial y}{\partial \alpha} &= \mu R \sin(\psi - \phi), \quad \frac{\partial y}{\partial \beta} = -\mu S \sin(\psi + \phi). \end{aligned} \tag{12}$$

The compatibility equations are

$$\frac{\partial^2 x}{\partial \alpha \partial \beta} = \frac{\partial^2 x}{\partial \beta \partial \alpha} \text{ and } \frac{\partial^2 y}{\partial \alpha \partial \beta} = \frac{\partial^2 y}{\partial \beta \partial \alpha}. \tag{13}$$

Substituting (13) into (12) and employing (9) yields

$$\begin{aligned} &\frac{\partial R}{\partial \beta}\cos(\psi - \phi) + \frac{\partial S}{\partial \alpha}\cos(\psi + \phi) - \mu\left[R\sin(\psi - \phi) + S\sin(\psi + \phi)\right] = 0, \\ &\frac{\partial R}{\partial \beta}\sin(\psi - \phi) + \frac{\partial S}{\partial \alpha}\sin(\psi + \phi) + \mu\left[R\cos(\psi - \phi) + S\cos(\psi + \phi)\right] = 0. \end{aligned} \tag{14}$$

These equations can be solved for the derivatives $\partial R / \partial \beta$ and $\partial S / \partial \alpha$. As a result,

$$\sin 2\phi \frac{\partial R}{\partial \beta} - \mu R \cos 2\phi - \mu S = 0 \text{ and } \sin 2\phi \frac{\partial S}{\partial \alpha} + \mu S \cos 2\phi + \mu R = 0. \tag{15}$$

Introduce R_0 and S_0 by the following relationships:

$$R = R_0 \exp(n\alpha + m\beta) \text{ and } S = S_0 \exp(n\alpha + m\beta), \tag{16}$$

where *n* and *m* are constant. Substituting (16) into (15) yields

$$\begin{aligned}\sin 2\phi\frac{\partial R_0}{\partial\beta}+\left(m\sin 2\phi-\mu\cos 2\phi\right)R_0-\mu S_0=0,\\ \sin 2\phi\frac{\partial S_0}{\partial\alpha}+\left(n\sin 2\phi+\mu\cos 2\phi\right)S_0+\mu R_0=0.\end{aligned} \tag{17}$$

Put

$$\mu=\sin 2\phi,\quad m=\cos 2\phi, \text{ and } n=-\cos 2\phi. \tag{18}$$

Then, equation (17) becomes

$$\frac{\partial R_0}{\partial\beta}-S_0=0 \text{ and } \frac{\partial S_0}{\partial\alpha}+R_0=0. \tag{19}$$

It is seen from these equations that R_0 and S_0 separately satisfy the equation of telegraphy. Methods of solving this equation in conjunction with typical boundary conditions adopted in plasticity theory are well-developed [2]. Also, equations (9) and (16) become

$$\Lambda-\Lambda_0=\left(\alpha-\beta\right)\sin 2\phi \text{ and } \psi=\left(\alpha+\beta\right)\sin 2\phi. \tag{20}$$

and

$$R=R_0\exp\left[\cos 2\phi\left(\beta-\alpha\right)\right] \text{ and } S=S_0\exp\left[\cos 2\phi\left(\beta-\alpha\right)\right]. \tag{21}$$

Using (21), one can rewrite (12) as

$$\begin{aligned}\frac{\partial x}{\partial\alpha}&=R_0\sin 2\phi\cos\left(\psi-\phi\right)\exp\left[\cos 2\phi\left(\beta-\alpha\right)\right],\\ \frac{\partial x}{\partial\beta}&=-S_0\sin 2\phi\cos\left(\psi+\phi\right)\exp\left[\cos 2\phi\left(\beta-\alpha\right)\right],\\ \frac{\partial y}{\partial\alpha}&=R_0\sin 2\phi\sin\left(\psi-\phi\right)\exp\left[\cos 2\phi\left(\beta-\alpha\right)\right],\\ \frac{\partial y}{\partial\beta}&=-S_0\sin 2\phi\sin\left(\psi+\phi\right)\exp\left[\cos 2\phi\left(\beta-\alpha\right)\right].\end{aligned} \tag{22}$$

Having (20) and a solution of the equations in (19), one can integrate the equations in (22) along any path in characteristic space.

4. STRENGTH OF A WELDED JOINT

Welded joints are an important class of structures. A distinguished feature of the highly under matched welded joints is that plastic yielding occurs in the weld, whereas the base material remains elastic at plastic collapse [23 - 25]. The simplest structure of this type is a welded panel subjected to tension (Figure 2). The thickness of the weld is 2*H*, and the width of the panel is 2 *W*. It is required to determine the distribution of the principal stresses along the center line of the weld. It is possible to assume without loss of generality that $H=1$.

The general structure of the characteristic net is shown in Figure 3. The characteristics of both families are straight in Region 1. Therefore, ψ and Λ are constant. The edge is traction-free. Therefore, $\sigma_2=0$ in Region 2.

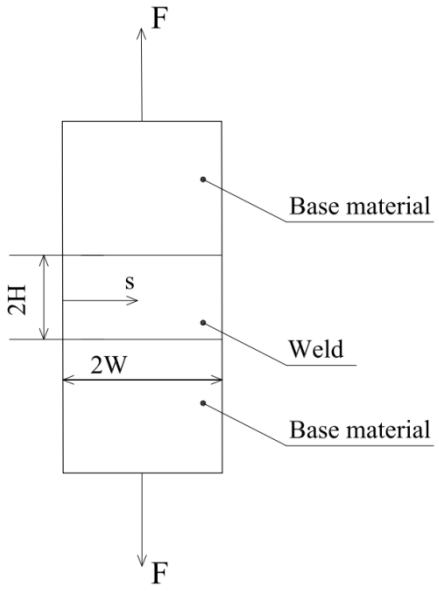

Figure 2. Schematic diagram of the tensile welded joint.

Then, it follows from (1) and (7) that

$$\sigma_1 = \frac{\sigma_0}{b} \text{ and } \Lambda = -\frac{\sqrt{q}}{(1-q)} \ln q \tag{23}$$

in Region 1. The direction of the principal stress σ_1 dictates the orientation of the characteristic lines. In particular, the base $\alpha-$ and $\beta-$ lines are shown in Figure 3. It is worthy of note that $\alpha = 0$ on the base $\beta-$ line and $\beta = 0$ on the base $\alpha-$ line. Choosing the Cartesian coordinate system shown in Figure 3 is convenient. In this case, $\psi = 0$ in Region 1.

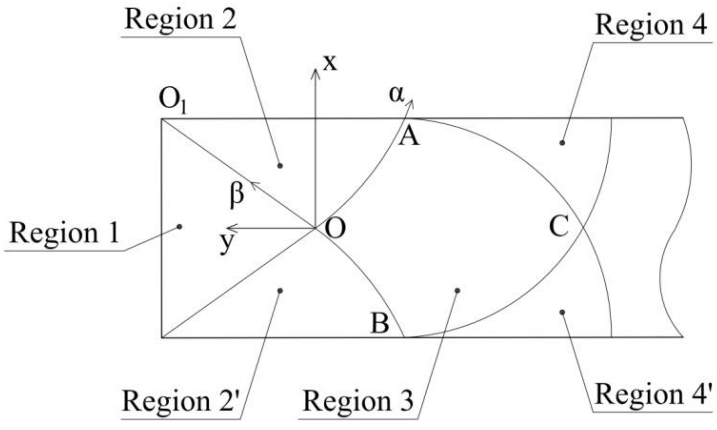

Figure 3. The general structure of the characteristic net.

Consider Region 2. The $\beta-$ lines are straight in this region. To construct the characteristic field on the right to the base $\alpha-$ and $\beta-$ lines employing the method developed in the previous

section, one must find the radii of curvature of these lines. To this end, it is convenient to use a polar coordinate system (r, θ). This coordinate system's origin is at point O_1 (Figures 3 and 4).

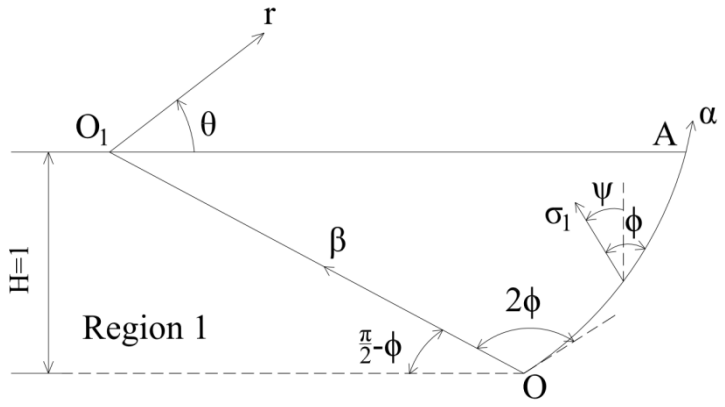

Figure 4. Characteristic and polar coordinates in Region 2.

Since the angle between the $\alpha-$ and $\beta-$ lines equals 2ϕ, the equation for a generic $\alpha-$line is

$$\frac{rd\theta}{dr} = \tan(\pi - 2\phi) = -\tan 2\phi. \tag{24}$$

The general solution of this equation is

$$\ln\frac{r}{r_0} = -\cot 2\phi(\theta - \theta_0), \tag{25}$$

where r_0 and θ_0 are constant. The base $\alpha-$line passes through point *O*. It is seen from the geometry of Figure 4 that the coordinates of this point are

$$r_0 = \frac{1}{\cos\phi} \text{ and } \theta_0 = \phi - \frac{\pi}{2}. \tag{26}$$

It follows from (25) and (26) that the equation of the base $\alpha-$line is

$$r = \frac{1}{\cos\phi}\exp\left[-\cot 2\phi\left(\theta - \phi + \frac{\pi}{2}\right)\right]. \tag{27}$$

The radius of curvature of this line is determined from the following equation:

$$|R_b| = \frac{\left(r^2 + r'^2\right)^{3/2}}{r^2 + 2r' - rr''}. \tag{28}$$

Here the subscript *'b'* emphasizes that it is the radius of curvature of the base $\alpha-$line. Moreover, $r' = dr/d\theta$ and $r'' = d^2r/d\theta^2$. It is seen from Figure 3 and equation (10) that $R_b > 0$. Therefore, substituting (27) into (28) gives

$$R_b = \frac{1}{\sin 2\phi \cos\phi} \exp\left[\left(\phi - \theta - \frac{\pi}{2}\right)\cot(2\phi)\right]. \tag{29}$$

It follows from the geometry of Figure 4 that

$$\psi = \theta - \phi + \frac{\pi}{2}. \tag{30}$$

Since $\beta = 0$ on the base $\alpha -$ line, the second equation in (20) transforms to

$$\psi = \alpha \sin 2\phi. \tag{31}$$

Equations (29), (30), and (31) combine to give

$$R_b = \frac{1}{\sin 2\phi \cos\phi} \exp\left[-\alpha \cos(2\phi)\right]. \tag{32}$$

Comparing (32) and the first equation in (21) at $\beta = 0$ shows that

$$R_0 = \frac{1}{\sin 2\phi \cos\phi} \tag{33}$$

for $\beta = 0$. It is seen from Figure 4 that $\theta = 0$ at point *A*. Then, it follows from (30) and (31) that

$$\alpha_A = \frac{\pi/2 - \phi}{\sin 2\phi}. \tag{34}$$

here α_A is the value of α at point *A*. The *y*-coordinate of this point is determined from the third equation in (22). In particular,

$$y_A = R_0 \sin 2\phi \int_0^{\alpha_A} \sin(\psi - \phi) \exp\left[\cos 2\phi(\beta - \alpha)\right] d\alpha. \tag{35}$$

Substituting $\beta = 0$, (31), and (33) into (35) and integrating, one gets

$$y_A = \tan\phi - \frac{1}{\cos\phi} \exp\left[\left(\phi - \frac{\pi}{2}\right)\cot 2\phi\right]. \tag{36}$$

Region 2' (Figure 3) can be treated similarly. As a result,

$$S_0 = -\frac{1}{\sin 2\phi \cos\phi} \tag{37}$$

for $\alpha = 0$,

$$\beta_B = -\frac{\pi/2 - \phi}{\sin 2\phi}, \tag{38}$$

and

$$y_B = \tan\phi - \frac{1}{\cos\phi} \exp\left[\left(\phi - \frac{\pi}{2}\right)\cot 2\phi\right]. \tag{39}$$

Here β_B and y_B are the $\beta -$ and $y -$ coordinates of point *B* (Figure 3), respectively.

Consider Region 3 (Figures 3 and 5). The characteristics of both families are curved in this region. Therefore, equation (19) is valid. The equations in (19) can be rewritten as

$$\frac{\partial R_0}{\partial\alpha\partial\beta}+R_0=0 \text{ and } \frac{\partial S_0}{\partial\alpha\partial\beta}+S_0=0. \tag{40}$$

Each of these equations is integrated by the method of Riemann. In particular, the Green's function is

$$G(a,b,\alpha,\beta)=J_0\left[2\sqrt{(a-\alpha)(b-\beta)}\right], \tag{41}$$

where $J_0(z)$ is the Bessel function of zero order. Note that

$$G(a,b,a,\beta)=1 \text{ and } G(a,b,\alpha,b)=1. \tag{42}$$

Using (33) and (37), one can integrate the equations in (19) along the base characteristics to get

$$S_0=-\frac{1+\alpha}{\sin 2\phi\cos\phi} \tag{43}$$

on OA' and

$$R_0=-\frac{\beta-1}{\sin 2\phi\cos\phi} \tag{44}$$

on OB'.

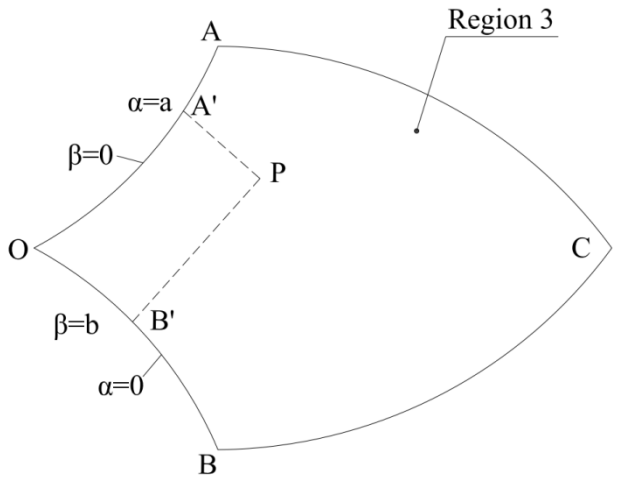

Figure 5. Representation of characteristic curves for Riemann's method of integration.

Assume one must find S_0 at point *P* (Figure 5). Consider closed contour *B'PA'OB'*. The method of Riemann leads to

$$\begin{aligned}\int_{B'P}\left(G\frac{\partial S_0}{\partial\alpha}-S_0\frac{\partial G}{\partial\alpha}\right)d\alpha+\int_{PA'}\left(S_0\frac{\partial G}{\partial\beta}-G\frac{\partial S_0}{\partial\beta}\right)d\beta+\\ \int_{A'O}\left(G\frac{\partial S_0}{\partial\alpha}-S_0\frac{\partial G}{\partial\alpha}\right)d\alpha+\int_{OB'}\left(S_0\frac{\partial G}{\partial\beta}-G\frac{\partial S_0}{\partial\beta}\right)d\beta=0.\end{aligned} \tag{45}$$

Consider the first two integrals .Since $\beta = b$ on $B'P$, it follows from (42) that $G = 1$ and $\partial G/\partial\alpha = 0$ in the integrand of the first integral. Therefore,

$$\int_{B'P}\left(G\frac{\partial S_0}{\partial\alpha} - S_0\frac{\partial G}{\partial\alpha}\right)d\alpha = \int_0^a \frac{\partial S_0}{\partial\alpha}d\alpha = S_P - S_{B'}, \tag{46}$$

where S_P is the value of S_0 at point P and $S_{B'}$ is the value of S_0 at point B'. The latter is given by (37). Then, equation (46) becomes

$$\int_{B'P}\left(G\frac{\partial S_0}{\partial\alpha} - S_0\frac{\partial G}{\partial\alpha}\right)d\alpha = S_P + \frac{1}{\sin 2\phi\cos\phi}. \tag{47}$$

The second integral in (45) can be treated similarly, except that (43) should be used instead of (37). As a result,

$$\int_{PA'}\left(S_0\frac{\partial G}{\partial\beta} - G\frac{\partial S_0}{\partial\beta}\right)d\beta = S_P + \frac{1+a}{\sin 2\phi\cos\phi}. \tag{48}$$

Integrating by parts and employing (41) and (43), one can represent the third integral in (45) as

$$\begin{aligned}\int_{A'O}\left(G\frac{\partial S_0}{\partial\alpha} - S_0\frac{\partial G}{\partial\alpha}\right)d\alpha &= \int_0^a\left[\frac{2G}{\sin 2\phi\cos\phi} + \frac{\partial(S_0G)}{\partial\alpha}\right]d\alpha = \\ \frac{2}{\sin 2\phi\cos\phi}\int_0^a J_0\left[2\sqrt{b(a-\alpha)}\right]d\alpha &- \frac{(1+a)}{\sin 2\phi\cos\phi} + \frac{1}{\sin 2\phi\cos\phi}J_0\left(2\sqrt{ab}\right).\end{aligned} \tag{49}$$

Substituting (37) into the fourth integral in (45) yields

$$\int_{OB'}\left(S_0\frac{\partial G}{\partial\beta} - G\frac{\partial S_0}{\partial\beta}\right)d\beta = -\frac{1}{\sin 2\phi\cos\phi}\int_0^b\frac{\partial G}{\partial\beta}d\beta = -\frac{1}{\sin 2\phi\cos\phi}\left[1 - J_0\left(2\sqrt{ab}\right)\right]. \tag{50}$$

Substituting (47) – (50) into (45) supplies

$$S_P = -\frac{1}{\sin 2\phi\cos\phi}\int_0^a J_0\left[2\sqrt{b(a-\alpha)}\right]d\alpha - \frac{1}{\sin 2\phi\cos\phi}J_0\left(2\sqrt{ab}\right). \tag{51}$$

Put $\chi = 2\sqrt{b(a-\alpha)}$. Then,

$$d\alpha = -\frac{\chi}{2b}d\chi. \tag{52}$$

Replacing integration with respect to α with integration with respect to χ in (51), one arrives at

$$S_P = \frac{1}{2b\sin 2\phi\cos\phi}\int_{2\sqrt{ab}}^0 \chi J_0(\chi)d\chi - \frac{1}{\sin 2\phi\cos\phi}J_0\left(2\sqrt{ab}\right). \tag{53}$$

It is known that

$$\chi J_0(\chi) = \frac{d\left[\chi J_1(\chi)\right]}{d\chi}, \tag{54}$$

where $J_1(\chi)$ is the Bessel function of the first order. Using (54), one can transform (53) to

$$S_P = \frac{1}{2b\sin 2\phi\cos\phi}\int_{2\sqrt{ab}}^{0} d\left[\chi J_1(\chi)\right] - \frac{1}{\sin 2\phi\cos\phi}J_0\left(2\sqrt{ab}\right) = \\ -\frac{1}{\sin 2\phi\cos\phi}\sqrt{\frac{a}{b}}J_1\left(2\sqrt{ab}\right) - \frac{1}{\sin 2\phi\cos\phi}J_0\left(2\sqrt{ab}\right). \tag{55}$$

Since $ab \le 0$, it is convenient to rewrite (55) as

$$S_P = -\frac{1}{\sin 2\phi\cos\phi}\left[\sqrt{\left|\frac{a}{b}\right|}I_1\left(2\sqrt{|ab|}\right) + I_0\left(2\sqrt{|ab|}\right)\right], \tag{56}$$

where $I_0(\chi)$ and $I_1(\chi)$ are the modified Bessel functions of zero and first orders, respectively.

The *y*-coordinate of point *P* can be determined from the fourth equation in (22) as

$$y = y_{A'} - \sin 2\phi\int_0^b S_P \sin(\psi+\phi)\exp\left[\cos 2\phi(\beta - a)\right]d\beta, \tag{57}$$

where $y_{A'}$ is the y-coordinate of point A' and ψ is found from (20) as

$$\psi = (a+\beta)\sin 2\phi. \tag{58}$$

The value of $y_{A'}$ is determined from the third equation in (22) at $\beta = 0$. As a result, with the use of (20) and (33),

$$y_{A'} = \frac{1}{\cos\phi}\int_0^a \sin(\alpha\sin 2\phi - \phi)\exp(-\alpha\cos 2\phi)d\alpha = \\ \tan\phi - \frac{\sin(\phi + a\sin 2\phi)}{\cos\phi}\exp(-a\cos 2\varphi). \tag{59}$$

Using (56), one can represent S_P involved in (57) as

$$S_P = -\frac{1}{\sin 2\phi\cos\phi}\left[\sqrt{\left|\frac{a}{\beta}\right|}I_1\left(2\sqrt{|a\beta|}\right) + I_0\left(2\sqrt{|a\beta|}\right)\right]. \tag{60}$$

Since $\alpha = -\beta$ at the symmetry axis, the *y*-coordinate of point *P* at this axis is found from (57) as

$$y = y_{A'} - \sin 2\phi\int_0^{-a} S_P \sin(\psi+\phi)\exp\left[\cos 2\phi(\beta - a)\right]d\beta. \tag{61}$$

Using (58) and (60), one can evaluate the integral involved in (61) numerically. This result and (59) provide the value of *y* at the symmetry axis. The parameter *a* varies in the range $0 \le \alpha \le \alpha_A$, where α_A is given in (34). The value of Λ at this point follows (20). Then, the stress σ_1 is determined from (7) and the stress σ_2 from (1). The continuity of the stresses across *AOB* and (24) require that

$$\Lambda_0 = -\frac{\sqrt{q}}{(1-q)}\ln q. \tag{62}$$

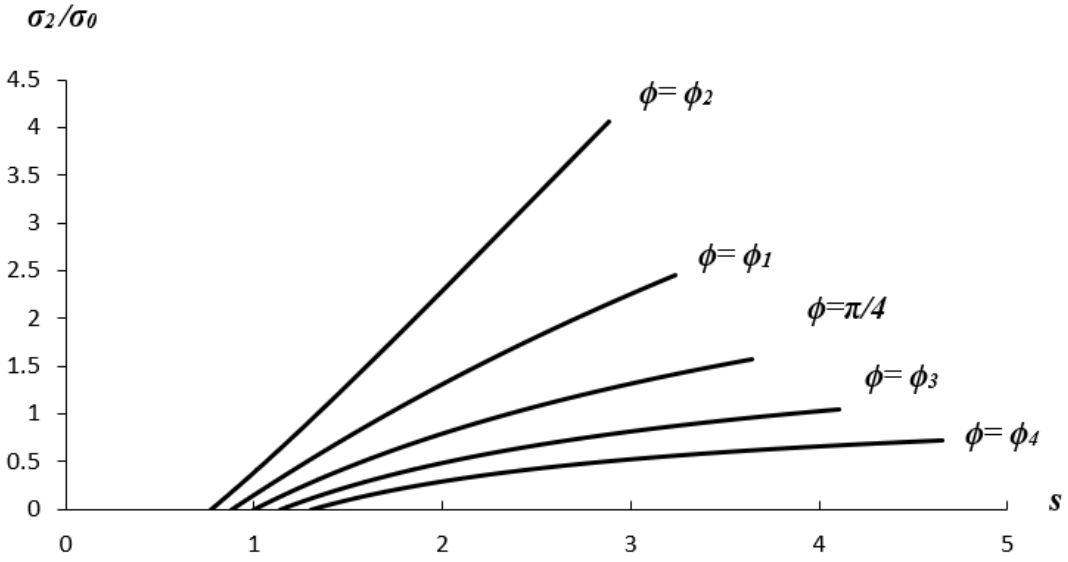

Figure 6. Distribution of the principal stress σ_1 along the center line of the welded joint.

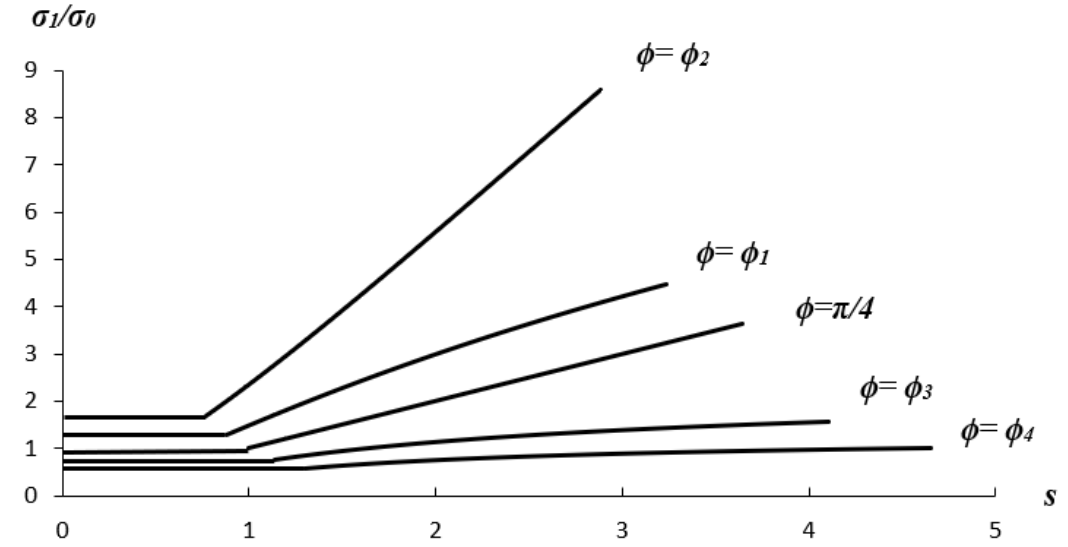

Figure 7. Distribution of the principal stress σ_2 along the center line of the welded joint.

Figures 6 and 7 illustrate the effect of ϕ on the distribution of the principal stresses along the center line. In these figures, *s* is the distance from the edge (Figure 2). It is seen from Figure 3 that

$$s = \tan\phi - y. \tag{63}$$

The curves in Figures 6 and 7 correspond to $\phi = \pi/4$ (pressure-independent material), $\phi = \phi_1 = \pi/4 - \pi/48$, $\phi = \phi_2 = \pi/4 - \pi/24$, $\phi = \phi_3 = \pi/4 + \pi/48$ and $\phi = \phi_4 = \pi/4 + \pi/24$.

The solution for pressure-independent material has been provided in [1]. The solution above reduces to this solution if $\phi = \pi/4$, which confirms its correctness.

4. CONCLUSIONS

The present paper has developed a general method for determining stress fields considering a generalized linear yield criterion. The method is applied to the models described by hyperbolic systems of equations. It has been shown that calculating stress fields in regions where both characteristic families are curved is reduced to solving the telegraph equation and several analytical relationships. A simple example illustrates the general method. In this case, a numerical procedure is only necessary to evaluate the ordinary integral in (61). Some numerical results are depicted in Figures 6 and 7. They show that the constitutive parameter involved in the yield criterion significantly affects the stress field at the center line of the tensile welded joint (Figure 2).

Acknowledgements. This publication has been supported by the RUDN University Scientific Projects Grant System, project No. 202247-2-000.

CRediT authorship contribution statement. Alexandrov S.: Methodology, Supervision. Rynkovskaya M.: Investigation, Funding acquisition. Bajmuratov I.: Formal analysis. Kalistratov R.: Investigation. Pylkin I.: Funding acquisition, Formal analysis.

Declaration of competing interest. The authors declare that they have no known competing financial interests or personal relationships that could have appeared to influence the work reported in this paper.

REFERENCES

1. Hill R., Lee E. H., Tupper S. J. - A method of numerical analysis of plastic flow in plane strain and its application to the compression of a ductile material between rough plates. Trans. ASME J. Appl. Mech. **18** (1951) 46-52.
2. Hill R. - The mathematical theory of plasticity, Clarendon Press, Oxford, 1950.
3. Thomason P. F. - Riemann-Integral solutions for the plastic slip-line fields around elliptical holes, J. Appl. Mech. **45** (1978) 678-679. https://doi.org/10.1115/1.3424381.
4. Sadowsky M. A. - Equiareal pattern of stress trajectories in plane plastic strain, ASME J. Appl. Mech. **63**(1941) A74-A76.https://doi.org/10.1115/1.4009104.
5. Cox G. M., Thamwattana N., McCue S. W., Hill J. M. - Coulomb–Mohr granular materials: quasi-static flows and the highly frictional limit, ASME Appl. Mech. Rev. **61** (6) (2008) 060802. https://doi.org/10.1115/1.2987874.
6. Liu P., Shen Y., Meng M., Luo S., Zhong Y., Cen Q. - Experimental study of mechanical properties and fracture characteristics of conglomerates based on Mohr–Coulomb criteria, J. Mar. Sci. Eng. **11** (6) (2023) 1219. https://doi.org/10.3390/jmse11061219.
7. Liu H., Liu J., Zhang S., Feng L., Qiu L. - Experimental study on compression characteristics of fractured soft rock and its Mohr-Coulomb criterion, Theor. Appl. Fract. Mech. **125** (2023) 103820. https://doi.org/10.1016/j.tafmec.2023.103820.
8. Yao N., Deng X., Luo B., Oppong F., Li P. - Strength and failure mode of expansive slurry-inclined layered rock mass composite based on Mohr–Coulomb criterion, Rock Mech. Rock Eng. **56** (2023) 3679-3692. https://doi.org/10.1007/s00603-023-03244-z.

9. Zhou J., Li C., Asteris P. G., Shi X., Armaghani D. J. - Chart-based granular slope stability assessment using the modified Mohr–Coulomb criterion, Arab. J. Sci. Eng. **48** (2023) 5549-5569. https://doi.org/10.1007/s13369-022-07478-x.
10. Tian D., Zheng H. - The generalized Mohr-Coulomb failure criterion, Appl. Sci. **13** (9) (2023) 5405. https://doi.org/10.3390/app13095405.
11. Zhao Y., Mishra B., Shi Q., Zhao G. - Size-dependent Mohr–Coulomb failure criterion, Bull. Eng. Geol. Environ. **82** (2023) 218. https://doi.org/10.1007/s10064-023-03243-y.
12. Zhang S., Wu X., Yang M., Ren P., Meng X. - Simulation of fracture performance of die-cast A356 aluminum alloy based on modified Mohr–Coulomb model, Appl. Sci. **13** (11) (2023) 6456. https://doi.org/10.3390/app13116456.
13. Druyanov B. - Technological mechanics of porous bodies, Clarendon Press, New York, 1993.
14. Altenbach H., Kolupaev V., Yu M. - Yield criteria of hexagonal symmetry in the π-plane, Acta Mech. **224** (2013) 1527-1540. https://doi.org/10.1007/s00707-013-0830-5.
15. Manola M. M. S., Koumousis V. K. - Ultimate state of plane frame structures with piecewise linear yield conditions and multi-linear behavior: a reduced complementarity approach, Comp. Struct. **130** (2014) 22-33. https://doi.org/10.1016/j.compstruc. 2013.09.003.
16. Alexandrov S. - Geometry of plane strain characterisctic fields in pressure-dependent plasticity, ZAMM **95** (11) (2015) 1296-1301. https://doi.org/10.1002/zamm.201400017.
17. Aleksandrov S. E., Lyamina E. A. - Riemann method for the plane strain of a homogeneous porous plastic material, Mech. Solids **50** (2) (2015) 171-175. https://doi.org/ 10.3103/S0025654415020065.
18. Alexandrov S. E., Lyamina E. A. - A new method of calculating the state of stress in granular materials under plane strain conditions, Transp. Syst. Technol. **3** (4) (2017) 89-106. https://doi.org/10.17816/transsyst20173489-106.
19. Alexandrov S., Rynkovskaya M., Tsai S. N. - Application of the generalized method of moving coordinates to calculating stress fields near an elliptic hole, Mater. **15** (2022) Article 6266. https://doi.org/10.3390/ma15186266.
20. Alexandrov S., Harris D. - Geometry of principal stress trajectories for a Mohr-Coulomb material under plane strain, ZAMM **97** (4) (2017) 473-476.
21. Alexandrov S., Date P. - A general method of stress analysis for a generalized linear yield criterion under plane strain and plane stress, Contin. Mech. Thermodyn. **31** (3) (2019) 841-849. https://doi.org/10.1007/s00161-018-0743-6.
22. Alexandrov S., Lyamina E., Jeng Y.-R. - A general stress solution in a plastic region near a traction-free boundary of arbitrary shape under plane-strain conditions, Contin. Mech. Thermodyn. **35** (2023) 121-139. https://doi.org/10.1007/s00161-022-01173-w.
23. Zerbst U., Madia M. - Analytical flaw assessment, Eng. Fract. Mech. **187** (2018) 316-367. https://doi.org/10.1016/j.engfracmech.2017.12.002.
24. Dilman V. L., Dheyab A. N. - Critical states of thin underlayers under tensile afford, J. Comput. Eng. Math. **5** (4) (2018) 3-15. DOI:10.14529/jcem180401.
25. Alexandrov S., Lyamina E., Jeng Y. R. - Effect of weld geometry on the limit load of a cracked specimen under tension, Mech. Based Des. Struct. Mach. (2023). https://doi.org/ 10.1080/15397734.2023.2165100.